TECHNICAL PAPER

Application of Desirability-Based Multiobjective Optimization Techniques to Study the Wear of Al Self-Lubricating Hybrid Nanocomposites

I. Manivannan[1] · S. Ranganathan[2] · S. Gopalakannan[3]

Abstract In this study, novel Al6061–SiC nanocomposites and Al6061–SiC–Gr hybrid nanocomposites were fabricated by ultrasonic cavitation method by adding silicon carbide (SiC) of 0.8 and 1.6% and graphite (Gr) of 0.5 and 1.0% by weight basis for each casting. A Three-level Box–Behnken design of experiment was developed using response surface methodology. Dry sliding wear tests were performed as per the experimental design using a pin-on-disc set-up at room temperature. Analysis of variance (ANOVA) was applied to investigate the influence of process parameters viz., load, sliding distance, wt% reinforcement and their interactions on specific wear rate and coefficient of friction. Further, a mathematical model was formulated by applying response surface method in order to estimate the tribology characteristics such as wear and COF of the hybrid nanocomposites. The specific wear rate and coefficient of friction were significantly influenced by % of SiC followed by % of Gr, load and sliding distance. The wear test parameters were optimized for minimizing specific wear rate and COF using desirability function approach. A set of optimum parameter of combination for AMMNC was identified as: SiC 1.36wt%; Gr 0.63 wt%; load 35.65 N and sliding distance 2848 m with specific wear rate of 0.517 g/N-m; coefficient of friction 0.181. The AFM image of Al6061–1.36SiC–0.63Gr hybrid nanocomposite at optimized condition confirmed the improvement in the wear surface smoothness of the hybrid nanocomposite compared to Al6061–SiC nanocomposites.

1 Introduction

Aluminium and its composites (AMCs) are one of the most widely used materials in aerospace and automotive industries. The high-performance tribological applications of aluminium alloy are limited in their use because of its poor wear resistance [1–3].The reinforcement of silicon carbide (SiC) and graphite (Gr) particles in aluminium leads to their superior wear resistance combined with a low friction coefficient. Graphite is widely used because of its ability to form film on metal, thereby lowering friction between the surfaces. However, graphite decreases the strength of the composite which can be compensated by the hard SiC nanoparticles present in the Al/SiC/Gr hybrid nanocomposites [4–7]. The development of Al/SiC/Gr self-lubricating hybrid nanocomposite is a novel material in the area of AMMNC$_S$ with improved mechanical and tribological properties. The use of these novel Al/SiC/Gr hybrid nanocomposite materials can improve energy efficiency, safety and reliability and also reduce oil consumption, power loss and maintenance cost [8–14].

✉ I. Manivannan
  i.manivannan72@gmail.com

  S. Ranganathan
  ranganathan.s@gmrit.edu.in

  S. Gopalakannan
  gopalakannan75@gmail.com

1 Department of Mechanical Engineering, Motilal Nehru Government Polytechnic College, Puducherry 605 008, India

2 Department of Mechanical Engineering, GMR Institute of Technology (An Autonomous Institution, Affiliated to JNTU, Kakinada), GMR Nagar, Rajam, Andhra Pradesh 532127, India

3 Department of Mechanical Engineering, Adhiparasakthi Engineering College, Melmaruvathur, Tamil Nadu 603 319, India

Wang et al. [15] established a novel method for dispersion of nanoparticles in molten metal by combined solidification process with ultrasonic cavitation. Ezatpour et al. [16] have successfully prepared $A7075/Al_2O_3$ nanocomposites with alumina powder of 0.4, 0.8 and 1.2 wt% by stir casting method followed by extrusion. The hardness, tensile and compression strength of nanocomposite is significantly improved compared to matrix alloy Al7075. Suresha and Sridhara have concluded that the addition of SiC and Gr particulates in Al–SiC–Gr hybrid composites significantly improved the tribological applications as it has low friction coefficient of 0.2 [17]. Mahdavi and Akhlaghi [18] reported that the hardness of Al–SiC–Gr hybrid composite increases as the SiC particle size decreases and also by reducing the graphite quantity the hardness increases. Hassan et al. [19] stated that increase in Gr increases the porosity of the composite which decreases the hardness. The addition of SiC as a second reinforcement in Al–Gr composites overcomes the demerits of Gr and improves the hardness of the composite. Kumar and Balasubramanian [20] developed a numerical model using RSM to forecast the abrasive wear rate of AA7075–SiC composite. The influence of volume % in reinforcement, reinforcement size, applied load and sliding speed on the wear behaviour of AA7075–SiC composite has been analysed, and it has been inferred that the reinforcement size exerts the greatest effect on wear. Basavarajappa et al. [21] fabricated Al–SiC–Gr hybrid composites by liquid metallurgy route, and the results of dry sliding wear of the hybrid composite were compared with that of Al–SiC composite. Using Taguchi technique, a set of experimental data for optimization was developed in a controlled manner. He concluded that wear of Al–SiC composite and Al–SiC–Gr hybrid composites is greatly affected by the sliding distance [21]. Sahin [22] developed Al-15 wt% SiC composite by powder metallurgy (PM) method and used analysis of variance (ANOVA) to examine the input parameters which affect the wear of the Al-15 wt% SiC composite. He stated that the abrasive wear is significantly affected by abrasive grain size followed by hardness. Suresha and Sridhara [23] developed Al–SiC–Gr hybrid composite by stir casting method and studied the tribological behaviour under dry sliding condition. Design of experiment (DOE) technique was employed to study the influence of parameters like load, sliding distance, sliding speed and % reinforcement. They concluded that load and sliding distance have positive effect on the wear of the hybrid composite [17]. In addition, various research works on the wear behaviour of hybrid AMCs and optimization have been done and reported [23–25].

However, the parametric studies on the dry sliding wear of AMMNCs are scarce. In this present work, an attempt is made to study the influence of process parameters viz.,

load, sliding distance, % reinforcement and their interactions on specific wear rate (SWR) and coefficient of friction (COF) of Al–SiC–Gr hybrid nanocomposite by using RSM.

2 Materials and Methods

2.1 Fabrication of Composites

Al6061–SiC nanocomposite and Al6061–SiC–Gr hybrid nanocomposite were fabricated by ultrasonic cavitation method by adding silicon carbide (SiC) of 0.8 and 1.6% and graphite (Gr) of 0.5 and 1.0% by weight basis on the basis of previous studies [6, 10]. The fabrication route and material properties have been described in our earlier work [6, 10].

2.2 Wear Test

The tribological studies were carried out on a computer integrated monitor (TR-20-PHM-M1 DUCOM) with an inbuilt load cell to measure the frictional force. For wear test, pins were machined to 10 mm diameter and 20 mm height. Disc surface of 25 mm diameter was maintained as sliding path. The tribotesting was carried out at three different normal loads (20 N, 30 N and 40 N). The sliding distances of 1000 m, 2000 m and 3000 m with sliding speed of 0.5 m/s were used. An electronic weighing balance was used for measurement of weight loss. The wear loss was calculated as the difference in weight of the samples before and after each test. The COF was directly recorded by a computer system connected to the wear test machine. The wear test procedure was followed according to ASTM G99 standard as has been discussed in our earlier work [6, 10].

3 Dry Sliding Wear Studies by Applying Response Surface Method

3.1 Experimental Design

RSM was used to find the relation between a set of input parameters and its output response. Design Expert-16 software was used to design the experiment and to study the effect of input parameters on SWR and COF of aluminium hybrid nanocomposite. In this study, four factors with three levels as shown in Table 1 have been used. Load, sliding distance, % reinforcement of SiC and % reinforcement of Gr were the input factors considered in this study. Table 2 shows the number of experiments to be conducted as per the experimental design matrix.

Table 1 Input levels of sliding wear parameters

Sl. no.	Parameter	Notation	Unit	Level		
				− 1	0	+ 1
1	wt% of SiC	A	%	0	0.8	1.6
2	wt% of Gr	B	%	0	0.5	1
3	Sliding distance	C	m	1000	2000	3000
4	Load	D	N	20	30	40

Table 2 Design factors and responses in coded form

Ex. no.	Run	% of SiC	% of Gr	Sliding distance (m)	Load	Specific wear rate $\times 10^{-7}$ (g/N-m)	Coefficient of friction (μ)
1	23	0.8	0	2000	40	1.15	0.311
2	26	0.8	0.5	2000	30	1.02	0.209
3	6	0.8	0.5	3000	20	0.89	0.219
4	14	0.8	1	1000	30	1.61	0.243
5	5	0.8	0.5	1000	20	1.52	0.226
6	10	1.6	0.5	2000	20	1.23	0.219
7	1	0	0	2000	30	2.72	0.55
8	19	0	0.5	3000	30	2.58	0.325
9	9	0	0.5	2000	20	2.65	0.356
10	12	1.6	0.5	2000	40	0.93	0.188
11	21	0.8	0	2000	20	1.48	0.338
12	17	0	0.5	1000	30	1.32	0.336
13	27	0.8	0.5	2000	30	1.02	0.209
14	8	0.8	0.5	3000	40	0.65	0.185
15	22	0.8	1	2000	20	1.26	0.245
16	29	0.8	0.5	2000	30	1.02	0.209
17	3	0	1	2000	30	1.51	0.288
18	24	0.8	1	2000	40	1.02	0.218
19	2	1.6	0	2000	30	1.36	0.317
20	7	0.8	0.5	1000	40	1.23	0.199
21	15	0.8	0	3000	30	1.32	0.317
22	4	1.6	1	2000	30	1.12	0.223
23	20	1.6	0.5	3000	30	0.78	0.193
24	18	1.6	0.5	1000	30	1.52	0.201
25	11	0	0.5	2000	40	1.98	0.211
26	13	0.8	0	1000	30	1.69	0.343
27	16	0.8	1	3000	30	0.93	0.228
28	28	0.8	0.5	2000	30	1.02	0.209
29	25	0.8	0.5	2000	30	1.02	0.209

Table 3 ANOVA for response surface quadratic model of specific wear rate

Source	Sum of square	Degree of freedom	Mean square	F-value	P value
Model	7	14	7.65	7.65	0.0002
A-SiC	2.82	1	2.82	43.18	< 0.0001
B-graphite	0.43	1	0.43	6.57	0.0225
C-sliding distance (m)	0.25	1	0.25	3.86	0.0696
D-load (N)	0.36	1	0.36	5.46	0.0348
AB	0.24	1	0.24	3.6	0.0787
AC	1	1	1	15.3	0.0016
AD	0.034	1	0.034	0.52	0.4812
BC	0.024	1	0.024	0.37	0.554
BD	2.03E−03	1	2.03E−03	0.031	0.8628
CD	6.25E−04	1	6.25E−04	9.56E−03	0.9235
A^2	1.73	1	1.73	26.53	0.0001
B^2	0.26	1	0.26	4	0.0652
C^2	0.023	1	0.023	0.35	0.5623
D^2	0.018	1	0.018	0.28	0.6035
Residual	0.92	14	0.065		
Lack of fit	0.92	10	0.092		
Pure error	0	4	0		
Cor total	7.92	28			

Standard deviation: 0.26, R^2: 0.8844, adjusted R^2: 0.7689 and predicted R^2: 0.3344

Table 4 ANOVA for response surface quadratic model of coefficient of friction

Source	Sum of squares	Degree of freedom	Mean square	F-value	P-value
Model	0.16	14	0.012	15.6	< 0.0001
A-SiC	0.044	1	0.044	58.77	< 0.0001
B-graphite	0.045	1	0.045	59.74	< 0.0001
C-sliding distance (m)	5.47E−04	1	5.47E−04	0.73	0.4062
D-load (N)	7.06E−03	1	7.06E−03	9.47	0.0082
AB	7.06E−03	1	7.06E−03	9.47	0.0082
AC	2.25E−06	1	2.25E−06	3.02E−03	0.957
AD	3.25E−03	1	3.25E−03	4.36	0.0556
BC	3.03E−05	1	3.03E−05	0.041	0.8432
BD	0	1	0	0	1
CD	1.23E−05	1	1.23E−05	0.016	0.8998
A^2	0.017	1	0.017	23.01	0.0003
B^2	0.04	1	0.04	53.17	< 0.0001
C^2	3.79E−05	1	3.79E−05	0.051	0.8249
D^2	6.60E−04	1	6.60E−04	0.88	0.3628
Residual	0.01	14	7.45E−04		
Lack of fit	0.01	10	1.04E−03		
Pure error	0	4	0		
Cor total	0.17	28			

Standard deviation: 0.027, R^2: 0.9398, adjusted R^2: 0.8795 and predicted R^2: 0.6531

4 Results and Discussion

4.1 Mathematical Model for SWR and COF

For analysis of SWR and COF, the quadratic model suggested from the fit summary is statistically significant. Tables 3 and 4 contain the ANOVA results of the quadratic models. When the value of Prob is less than 0.05 (i.e., $\alpha = 0.05$ or 95% confidence), the obtained models are statistically significant, which is desirable as it demonstrates the terms in the model that have a significant effect on the responses. When Prob is more than 0.05, the model is insignificant [26]. When the value of R^2 approaches unity, the difference between actual and predicted data is very less, which means that the response model fits the actual data. Further, if adequate precision (AP) is greater than 4, the predicted value can be compared with the average prediction error at the design point. Such model can be used to navigate the design space. Signal-to-noise ratio discriminates the adequate model if the value is greater than 4. These developed models have higher (R^2) and (AP) values. The values obtained are as follows: $R^2 = 0.8844$ and $AP = 11.899$ for SWR; $R^2 = 0.9398$ and $AP = 16.976$ for COF. Subsequently, these mathematical models developed for SWR and COF are considered to be significant for fitting and forecasting the experimental results. At the same time, test of lack of fit must be insignificant. The insignificant terms are removed by backward elimination process to fit into the quadratic models [26]. After backward elimination process, the response equations of SWR and COF of the final quadratic models are presented below.

$$\text{Specific wear rate (g/N - m)} = +1.02 - 0.48 * A - 0.19 * B - 0.17 * D + 0.24 * A * B + 0.092 * A * D + 0.023 * B * D$$

$$\text{Coefficient of friction } (\mu) = +0.52 * A^2 + 0.20 * B^2 + 0.053 * D^2 - 0.21 - 0.060 * A - 0.061 * B - 0.024 * D + 0.042 * A * B + 0.028 * A * D + 0.000 * B * D + 0.051 * A^2 + 0.078 * B^2 - 0.010 * D^2.$$

4.2 Effect of Dry Sliding Parameters on SWR

The surface graph in Fig. 1a–e shows the influence of % of SiC and Gr on SWR of Al6061–SiC–Gr hybrid nanocomposites for the applied load of 20–40 N and sliding distance of 1000–3000 m. It is observed that when the applied load increases, the SWR decreases due to the formation of mechanically mixed layer (MML). On comparing all the nanocomposites, when the SiC % is increased, SWR decreases up to 1.2% and increases for 1.6%. The increase in SWR is due to more agglomeration at 1.6% of SiC. The SWR decreases due to increase in hardness of Al–SiC nanocomposites for all applied load. This is due to the fact that the hard SiC nanoparticles on reinforcement with Al6061 matrix alloy create good interfacial bonding, which improves the hardness and strength of the nanocomposite. During sliding, the SiC particles act as load bearers and protect the soft matrix alloy from wear and it results in the improvement of wear resistance of the nanocomposite. The wear trend of the present work is consistent with Sameezadeh, Mosleh-shirazi and Akhlaghi [11, 12].

The SWR decreases with increase in SiC and attains a minimum at 1.2% SiC with 0.5% Gr. This is comparatively less than that of the alloy and Al6061–SiC nanocomposite. The soft graphite particle acts as a lubricant in the Al6061–SiC–0.5Gr hybrid nanocomposite. The graphite particle results in the creation of uniform lubricating film on the tribolayer of the hybrid nanocomposites. This leads to the decrease in SWR of Al–SiC–Gr hybrid nanocomposite. The SWR of Al6061–SiC–1.0Gr hybrid nanocomposite decreases with increase in SiC up to 1.2%. But the SWR of Al6061–SiC–1.0Gr hybrid nanocomposite is high compared to Al6061–SiC–0.5Gr hybrid nanocomposite. When Gr % is increased to 1.0%, agglomeration of particles increases and hardness of the hybrid nanocomposite decreases, which increases the SWR. These findings are consistent with Mosleh-Shirazi and Akhlaghi [13]. The SWR is significantly influenced by % SiC followed by %Gr.

4.3 Effect of Dry Sliding Parameters on COF

Figure 2a–e shows the effect of load, sliding distance, and % of SiC and Gr on COF of Al–SiC–Gr hybrid nanocomposite. It is noted that COF decreases when load is increased from 20 to 40 N. Due to the formation of tribolayer in Al–SiC–Gr hybrid nanocomposites at high load, friction between pin and disc get reduced resulting in decreased COF compared to Al–SiC nanocomposites and Al6061 matrix alloy. The existence of a stable tribolayer at the point of contact is the key factor in reducing the COF of hybrid nanocomposite independent of sliding distance. The COF value decreases as the % of SiC increases up to 1.2%, but the COF increases beyond 1.2% of SiC. Similarly, the COF gradually decreases on increasing the % of graphite up to 0.5% beyond which there is increase in the COF. The observations are consistent with Mosleh-Shirazi and Akhlaghi [13]. The COF is significantly influenced by % SiC followed by % Gr, load and sliding distance.
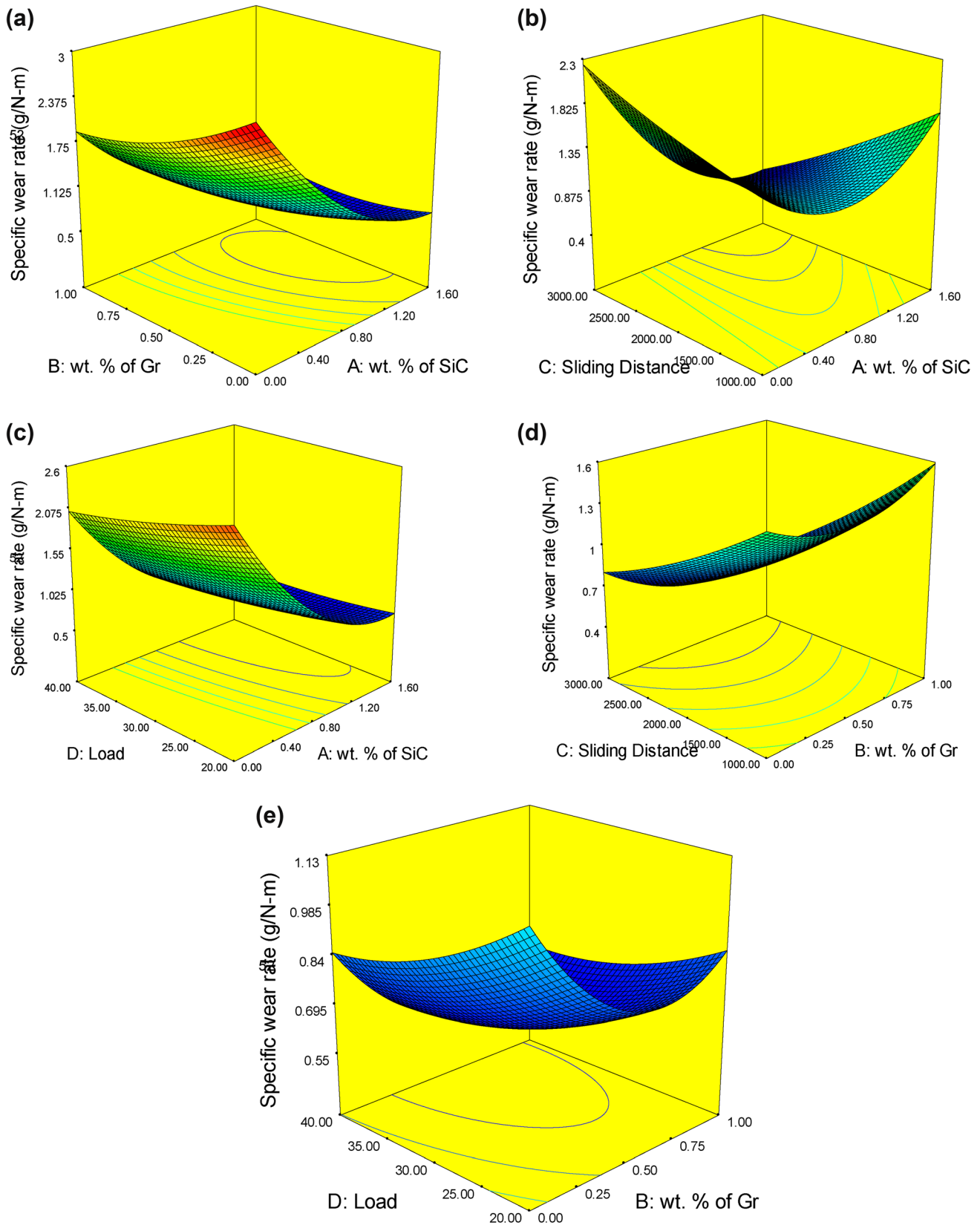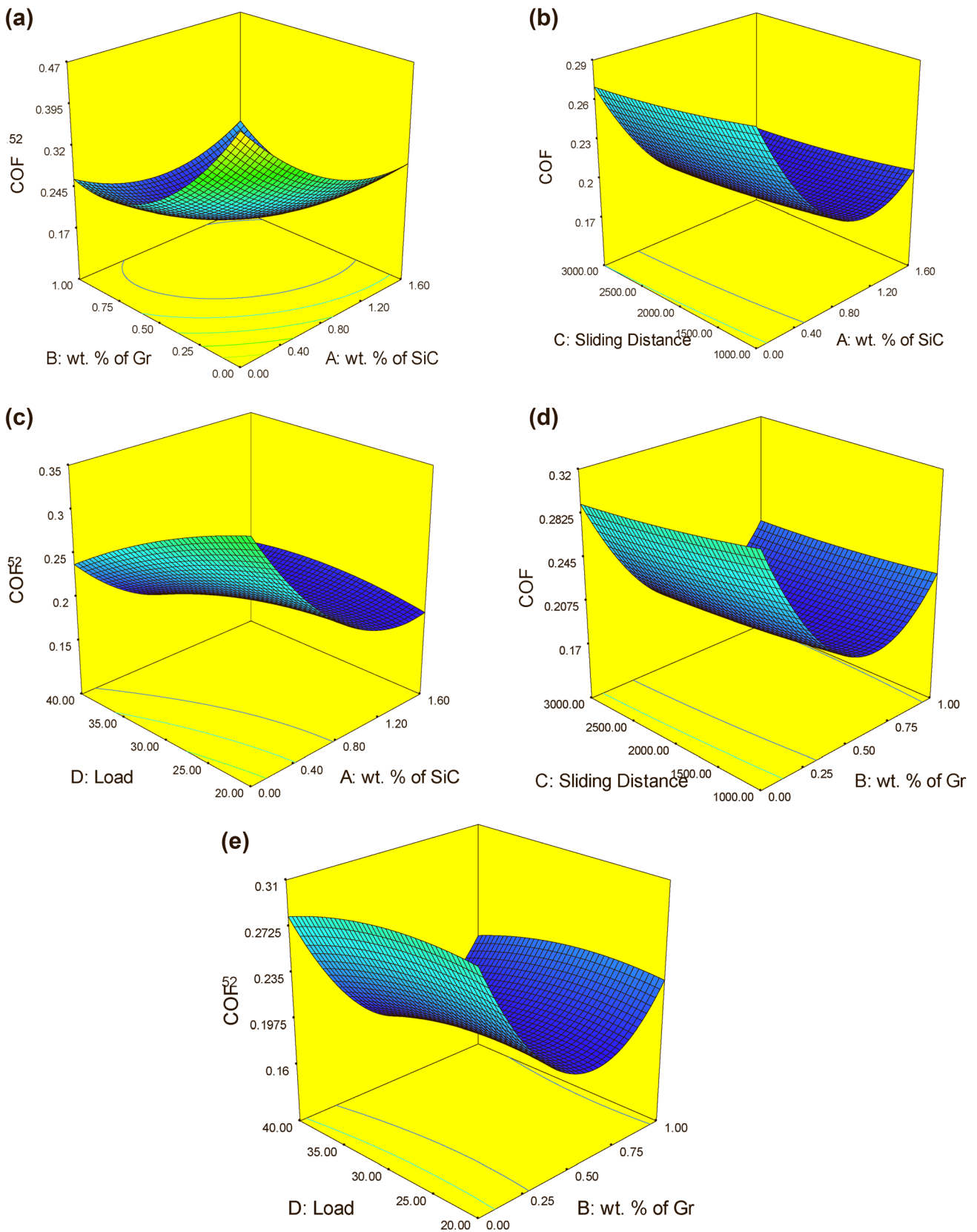
Fig. 1 3D interaction plot for specific wear rate (**a**, **b**, **c**, **d**, **e**)

Fig. 2 3D interaction plot for coefficient of friction (**a**, **b**, **c**, **d**, **e**)

4.4 Worn Surface Analysis for Various Nanocomposites

The morphology of the wear surface of Al6061 matrix, Al6061–0.8 SiC nanocomposite and Al–0.8SiC–0.5Gr hybrid nanocomposite pin tested at load of 20 N, 30 N and 40 N is shown in Fig. 3a–g. The SEM image provides valuable information about the wear mechanism of alloy, nanocomposite and hybrid nanocomposite. On increasing the load to 40 N, abrasive wear decreases and adhesive wear increases, which is clearly identified by big sized wear debris as shown in Fig. 3a. The dominating wear mechanisms of Al6061 are abrasive and adhesive wear.

Figure 3b shows the worn surface of Al–0.8SiC nanocomposite at the applied load of 20 N. The SEM image shows parallel and less deep grooves due to abrasive wear. Figure 3c shows the worn surface of Al–0.8SiC nanocomposite at the applied load of 40 N. It is observed that deep craters are formed on the worn surface of the nanocomposite which indicates that abrasive wear is dominant at high load. The worn surfaces of Al6061–0.8SiC nanocomposite possess less plastic deformation when compared to the wear surface of matrix alloy. Based on the Archard's equation

$$V = KWS/3H$$

where V is the volume loss, K is the wear coefficient and represents the wear intensity, S is the sliding distance, and H is the hardness. The increased hardness improves the resistance of the nanocomposite material against plastic deformation and decreases wear rate. The enhanced wear resistance of nanocomposite materials as compared with that of monolithic alloy is due to an increase in the thermal stability of the aluminium matrix because of the addition of SiC particles [12]. The most important factor is the presence of hard SiC particles in the soft matrix alloy, which prevent the matrix from sliding wear and strengthen the matrix. Moreover, these SiC particles restrict the dispersion and cutting of the disc into nanocomposite surface, thereby preventing delamination. In addition, the wear debris formed during dry sliding gets oxidized and forms a
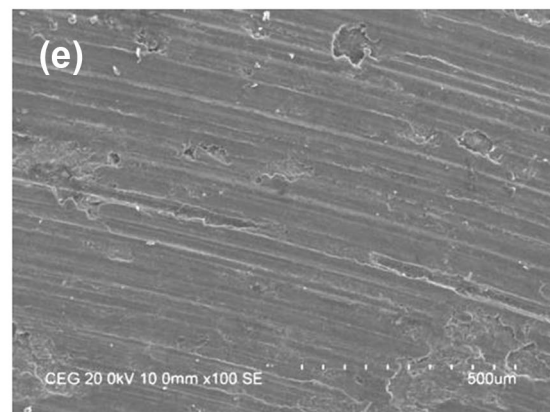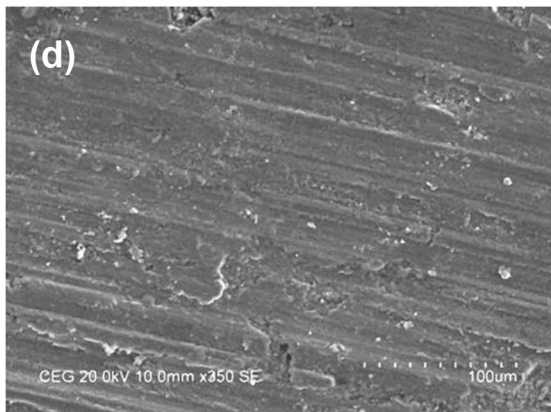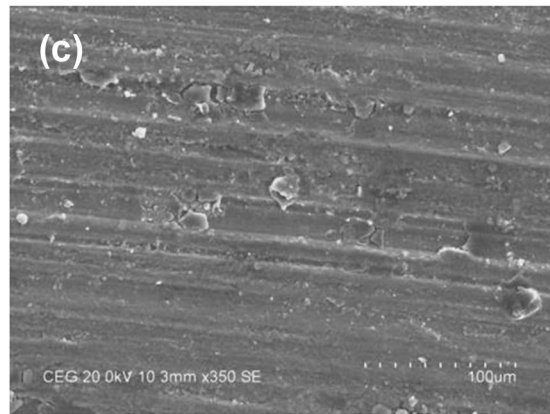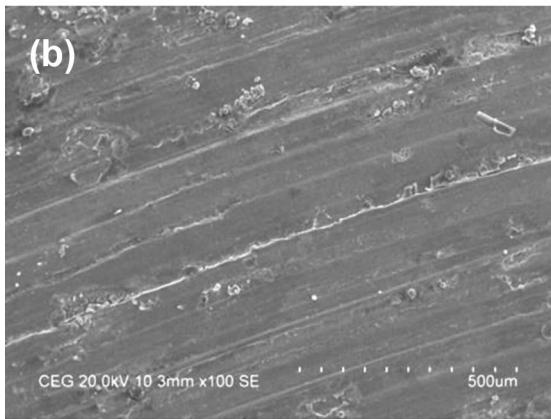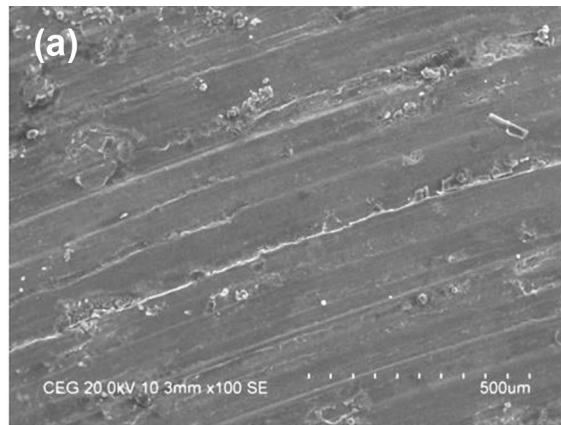
Fig. 3 SEM of worn surfaces of **a** Al6061 D 2000 m L 30 N, **b** Al–0.8SiC D 2000 L 20 N, **c** Al–0.8SiC D 2000 L 40 N, **d** Al–0.8SiC–0.5Gr D 3000 m L 20 N, **e** Al–0.8SiC–0.5Gr 1000 L 40 N, **f** Al–0.8SiC–1.0Gr D 2000 m L 20 N and **g** Al–0.8SiC–1.0Gr D 2000 m L 40 N. (L load, D sliding distance)

protective layer called mechanically mixed layer (MML) on the surface of nanocomposites.

Figure 3d shows the SEM image of wear surface of Al–0.8SiC–0.5Gr hybrid nanocomposite under applied load of 20 N. It indicates parallel and shallow grooves which is a confirmation of abrasive wear. In Fig. 3e, shallow craters are observed on the wear surface of Al–0.8SiC–0.5Gr hybrid nanocomposite at 40 N load, which indicates that abrasive wear is less operative at high load. Consequently, oxidation and delamination are dominant wear mechanisms in Al–0.8SiC–0.5Gr hybrid nanocomposite. The worn surface of 0.8SiC–0.5Gr hybrid nanocomposite appears smooth, compared to Al6061–0.8SiC nanocomposite and Al6061 matrix alloy. The tribolayer findings are consistent with Manivannan et al., Mosleh-Shirazi and Akhlaghi, Ravindran et al. [10, 13, 23].

Figure 4a–c shows the cross-sectional SEM micrographs of the wear track of Al6061 and Al6061–0.8SiC and confirm the presence of MML. This hard MML acts as lubricant and reduces the friction between the disc and the pin surface which reduces the wear and COF of the nanocomposite. Comparing the cross-sectional SEM micrographs shown in Fig. 4d, e of the wear track of Al6061 and Al6061–0.8SiC–0.5Gr confirms the presence of tribolayer. The graphite particle in the tribolayer forms a lubricating layer on worn surface of Al–SiC–Gr hybrid nanocomposite which restricts the formation of grooves.

Figure 5 shows the AFM images of worn surfaces of (a) Al6061 D 2000 m L 30 N (b) Al–0.8SiC D 2000 L 20 N (c) Al–0.8SiC D 2000 L 40 N (d) Al–0.8SiC–0.5Gr D 3000 m L 20 N (e) Al–0.8SiC–0.5Gr D 1000 L 40 N (f) Al–0.8SiC–1.0Gr D 2000 m L 20 N (g) Al–0.8SiC–1.0Gr D 2000 m L 40 N (L load, D sliding distance). The results of AFM analysis match with wear examinations and
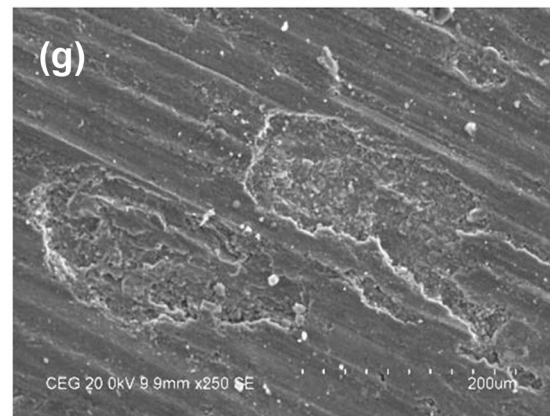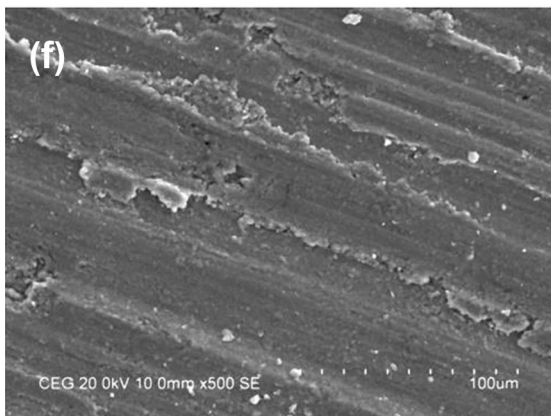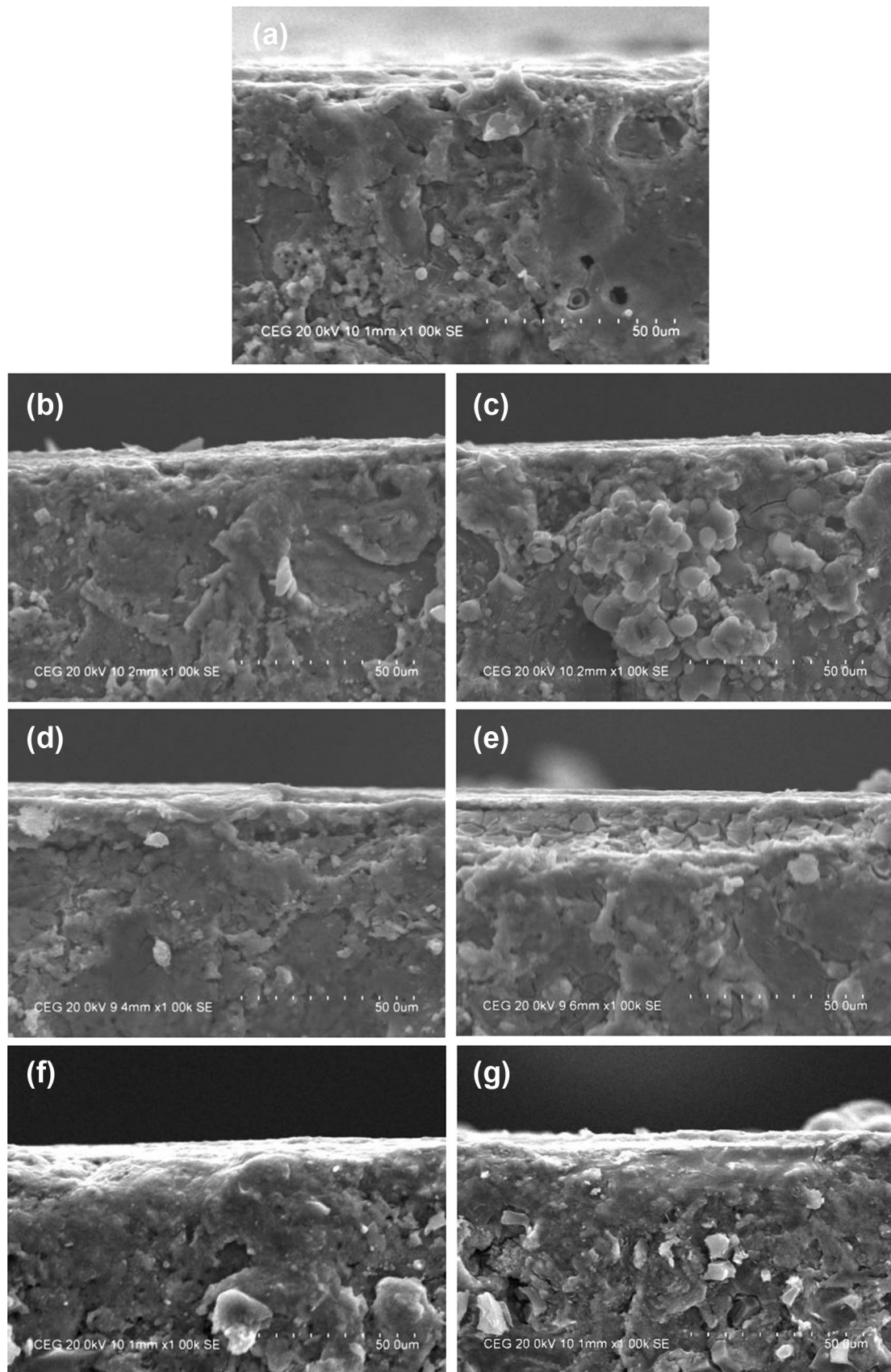
◄**Fig. 4** Cross-sectional SEM of the wear track of **a** Al6061 D 2000 m L 30 N, **b** Al–0.8SiC D 2000 L 20 N, **c** Al–0.8SiC D 2000 L 40 N, **d** Al–0.8SiC–0.5Gr D 3000 m L 20 N, **e** Al–0.8SiC–0.5Gr D 1000 L 40 N, **f** Al–0.8SiC–1.0Gr D 2000 m L 20 N and **g** Al–0.8SiC–1.0Gr D 2000 m L 40 N. (L load, D sliding distance)

the above said morphologies of worn surfaces. The AFM image of Al–0.8SiC–0.5Gr D 1000 L 40 N exhibits relatively smooth surface after wear compared to nanocomposites and matrix alloy. The worn surface of Al6061 indicates rough surface compared to nanocomposites and hybrid nanocomposites.

4.5 EDS of Wear Worn Surfaces

The results of EDS of worn surface of alloy, nanocomposite and hybrid nanocomposite after wear test under 40 N load are shown in Fig. 6a–c. Figure 6a shows the EDS analysis of the worn surface of Al6061 alloy. It majorly contains aluminium which indicates that the base alloy wear is more compared to the disc surface. The MML formation due to the oxidation of iron and aluminium wear debris of the nanocomposite is confirmed by the EDS analysis of Al6061–0.8SiC nanocomposite shown in Fig. 6b. The hard MML lowers the SWR of the nanocomposite compared to Al6061 alloy [12]. Figure 6c is the graph corresponding to Al–0.8SiC–0.5Gr hybrid nanocomposite, which confirms the presence of tribolayer containing iron, aluminium, carbon and its oxide. The SWR of the hybrid nanocomposite decreases due to high amount of iron (Fe) and graphite particles on the wear worn surface. The carbon peak shows that the graphite particles act as solid lubricant forming a tribolayer at the contact surface. The oxide peak indicates the formation of a protective oxide layer on the worn surface of the hybrid nanocomposite. Similar findings are observed by Mosleh-shirazi and Akhlaghi and Ravindran et al. [13, 23].

4.6 Multiresponse optimization of Al6061–SiC–Gr

It is important to identify the optimum parameters for any process. It is difficult to select the optimum condition for

SWR and COF of Al6061–SiC–Gr during dry sliding since it involves lot of process variables. Multiresponse tribological parameters are optimized using grey relational analysis, artificial neural networks with genetic algorithms, Taguchi's method and desirability function approach. The desirability function approach is extensively used for optimization of multiresponse parameter in industry [27–29]. The value of desirability is evaluated using Design Expert software. RSM develops a set of data depending on input parameters to optimize the SWR and COF. The aim of optimization is to find the input parameters which minimize SWR and COF.

The various process parameters, its goal, upper and lower limit and its optimum value of input parameters (load, distance, % of SiC and Gr) and output parameters (SWR and COF) are listed in Table 1. Out of various set of input conditions, the one with highest desirability is chosen as optimum condition and it is shown in Figs. 7 and 8. A dot on each ramp indicates response prediction for that parameter. The overall desirability function of SWR and COF is shown in the bar graph of desirability. The range of desirability value is from 0 to 1. When the desirability value is close to 1, it indicates the closeness of the target. The set of parameters for optimization is as follows: SiC 1.36 wt%; and Gr 0.63 wt%; load 34.65 N and sliding distance 2848 m; with specific wear rate of 0.517 g/N-m; coefficient of friction 0.181.

4.7 SEM and AFM Image for Optimization Confirmation

The SEM and AFM analysis of the worn surface of Al6061–1.36SiC–0.63Gr at optimum condition has been used to check the accuracy of the model. Figure 9a shows the worn surface at optimum conditions: load, 34.65 N; sliding distance, 2848 m. It is observed that only small scratches are seen at few places of the worn surface, which is an indication of low SWR. It confirms the accuracy of the model. Figure 9b shows the 3D AFM image of the Al–SiC–Gr hybrid nanocomposite. The height of the groove indicates the roughness of the surface. Lower the height is, lower will be the surface roughness. It is clear from the AFM image that at the optimum % of SiC and Gr particles
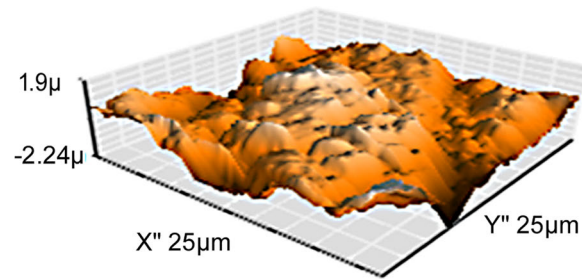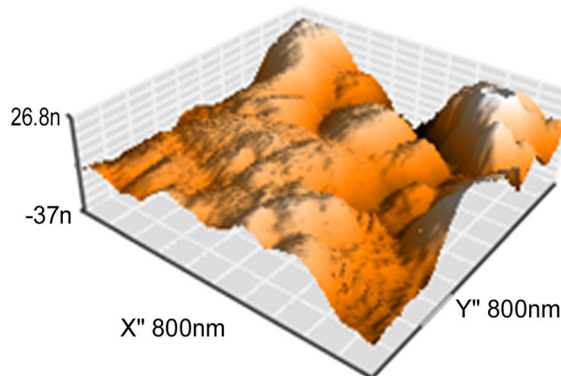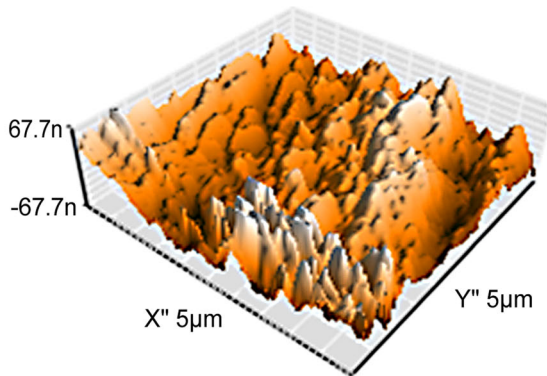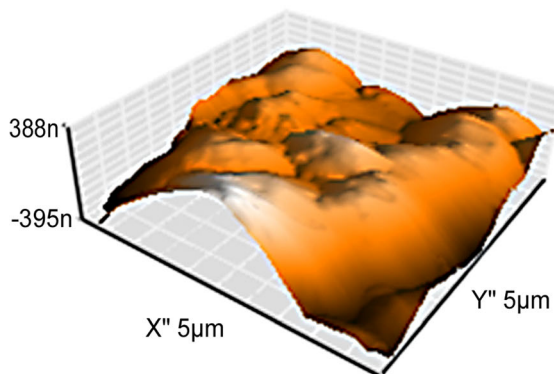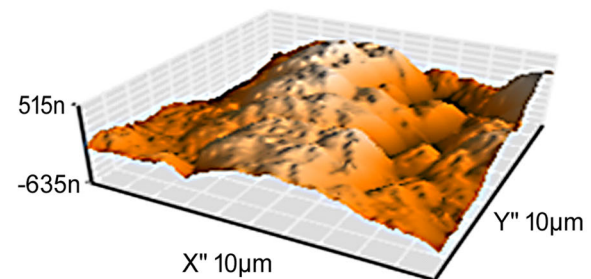
(a)
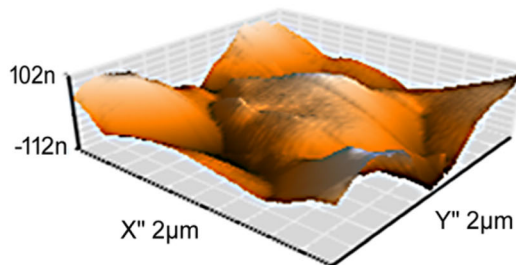
(b)
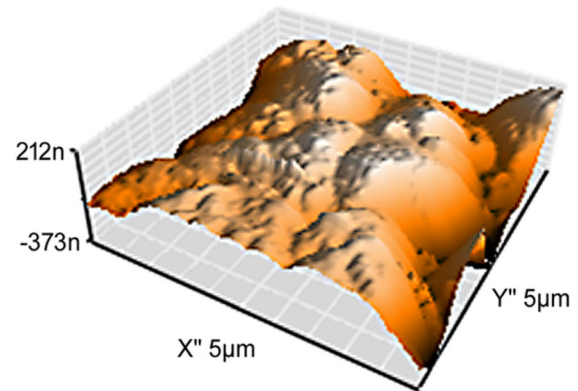
(c)

(d)

(e)

(f)

(g)

◄**Fig. 5** AFM (3D) of **a** Al6061 D 2000 m L 30 N, **b** Al–0.8SiC D 2000 L 20 N, **c** Al–0.8SiC D 2000 L 40 N, **d** Al–0.8SiC–0.5Gr D 3000 m L 20 N, **e** Al–0.8SiC–0.5Gr D 1000 L 40 N, **f** Al–0.8SiC–1.0Gr D 2000 m L 20 N and **g** Al–0.8SiC–1.0Gr D 2000 m L 40 N. (L load, D sliding distance)
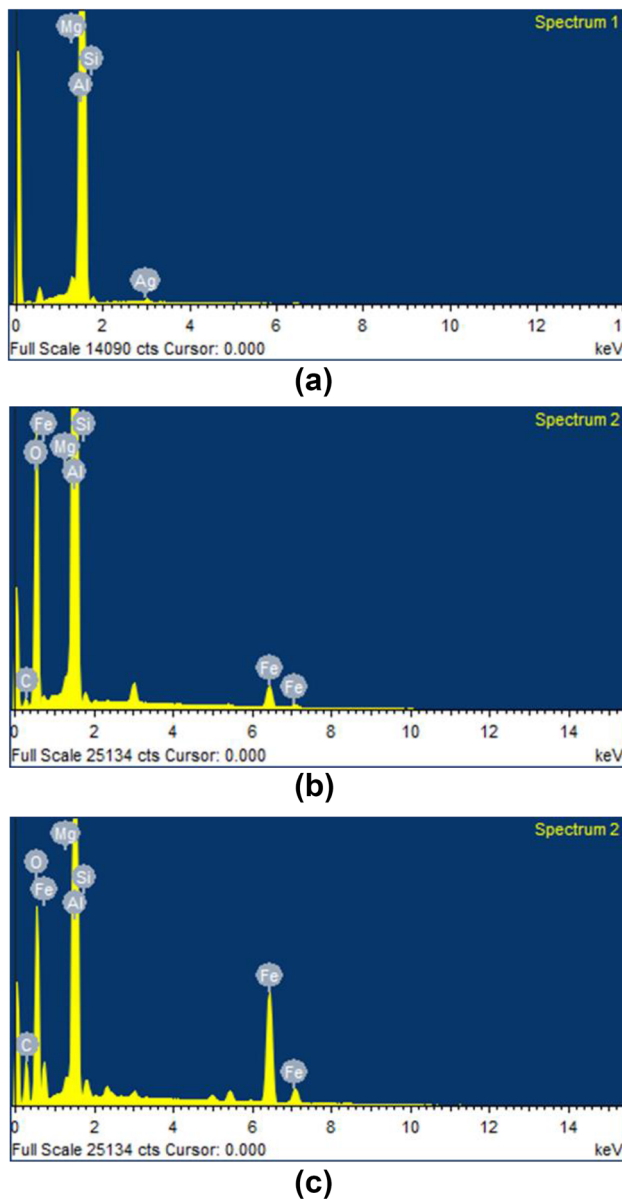

(a)

(b)

(c)

Fig. 6 EDS results of wear worn surface for various composites and hybrid composite under 40 N load: **a** Al6061, **b** Al6061–0.8 SiC and **c** Al6061–0.8 SiC–0.5Gr

in the hybrid nanocomposite, there is decrease in groove height indicating the smoothness of the worn surface.

5 Conclusion

In the present research work, aluminium-based metal matrix nanocomposites and hybrid nanocomposites reinforced with nano-sized SiC and Gr particles were successfully fabricated by ultrasonic cavitation method. The dry sliding wear of Al–SiC nanocomposites and Al–SiC–Gr hybrid nanocomposites were successfully carried out using Box–Behnken design of experiments of RSM by conducting 29 experiments for four factors at three levels.

The influence of process parameters on SWR and COF of Al–SiC nanocomposites and Al–SiC–Gr hybrid nanocomposites was investigated. A mathematical model was developed to predict the SWR and COF of Al–SiC nanocomposites and Al–SiC–Gr hybrid nanocomposites incorporating the effects of % reinforcement SiC and Gr, applied load and sliding distance. The predicted values matched the experimental values reasonably well with R^2 of SWR and COF.

ANOVA was used to check the adequacy of the model. The test results showed minimum deviation between actual value and predicted value which confirmed the accuracy of the developed model. The SWR and COF were significantly influenced by % SiC followed by % Gr, load and sliding distance.

The parameters were optimized using desirability-based multiresponse optimization technique to minimize the SWR and COF. The optimum parameters of combination setting for Al–SiC–Gr hybrid nanocomposites obtained were SiC of 1.36 wt%, Gr of 0.63 wt%, load of 34.65 N, sliding distance of 2848 m for minimizing SWR and COF.

The AFM image of Al6061–1.36SiC–0.63Gr hybrid nanocomposite at optimized condition confirmed the improvement in the wear surface smoothness of the hybrid nanocomposite compared to Al6061–SiC nanocomposites.
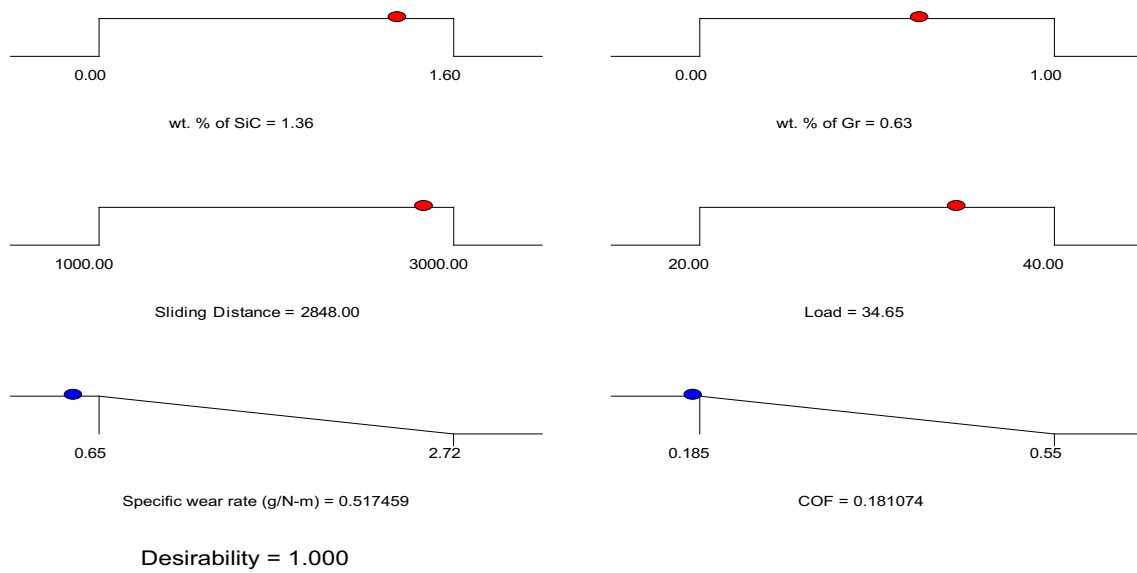
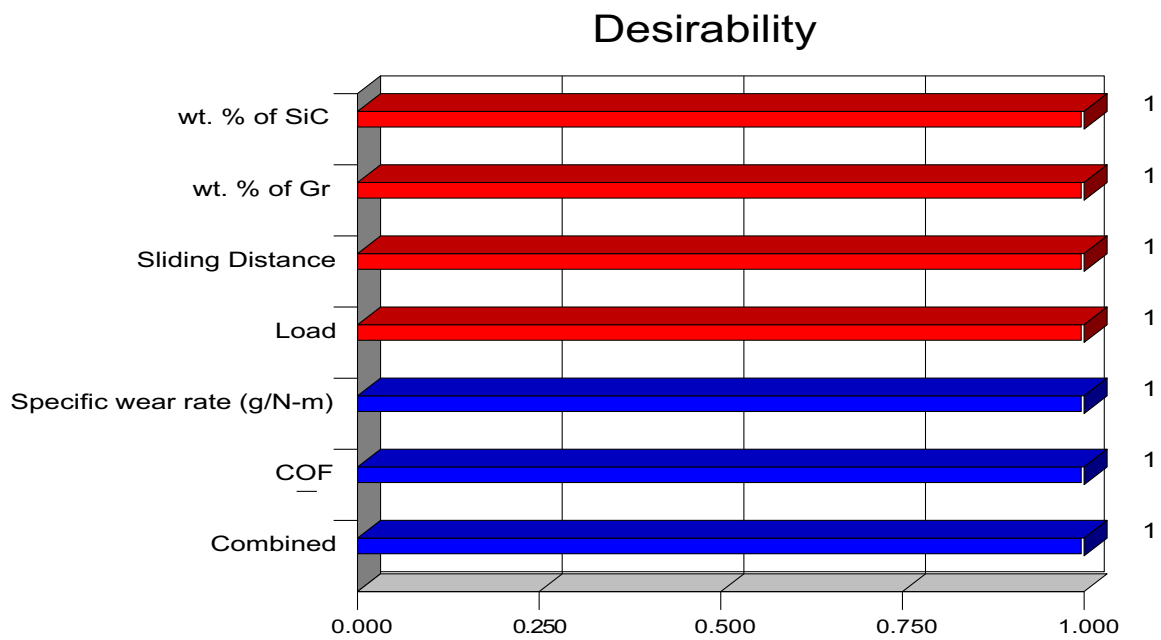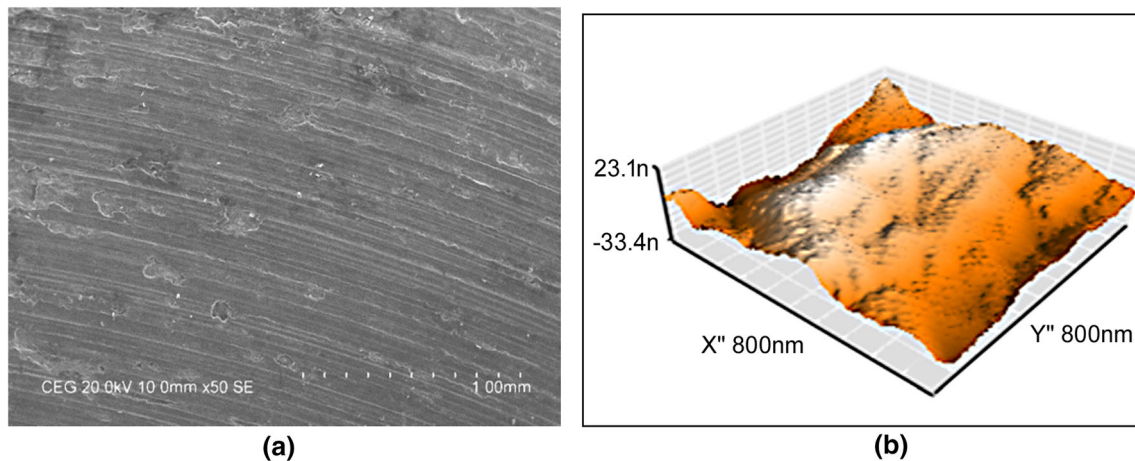**Fig. 7** Ramp function graph of desirability

Fig. 8 Bar graph of desirability

Fig. 9 **a** SEM of Al–1.36SiC–0.63Gr worn surface and **b** AFM of Al–1.36SiC–0.63Gr worn surface

References

1. Rohatgi P K, Schultz B F, Daoud A, and Zhang W W, *Tribol Int* **43** (2010) 455.
2. Vencl A, Bobic I, Arostegui S, Bobic B, Marinkovic A, and Babic M, *J Alloys Compd* **506** (2010) 631.
3. Mahdavi S, and Akhlaghi F, *J Mater Sci* **464** (2011) 7883.
4. Ravindran K, Manisekar P, Narayanasamy N, Selvakumar R, and Narayanasamy R, *Mater Des* 39 (2012) 42.
5. Sajjadi S A, Ezatpour H R, and Beygi H, *Mater Sci Eng A* **528** (2011) 8765.
6. Manivannan I, Ranganathan S, Gopalakannan S, Suresh S, Nagakarthigan K, and Jubendradass R, *Surface Interfaces* **8** (2017) 127.
7. Li J, Lu S, Wu S, Guo W, and Li F, *J Alloys Compd* **769** (2018) 848.
8. Yang Y, Lan J, and Li X, *Mater Sci Eng A* **380** (2004) 378.
9. Eskin G I, and Eskin D G, *Ultrason Sonochem* **10** (2003) 297.
10. Manivannan I, Ranganathan S, Gopalakannan S, and Suresh S, *Trans Indian Inst Met* **71** (2018) 1897.
11. Sameezadeh M, Emamy M, and Farhangi H, *Mater Design* **32** (2011) 2157.
12. Mosleh-shirazi S, and Akhlaghi F, *Tribol Int* **102** (2016) 28.
13. Mosleh-Shirazi S, Akhlaghi F, and Li D Y, *Tribol Int* **103** (2016) 620.
14. Mohammad Sharif E, Karimzadeh F, and Enayati M H, *Mater Des* **32** (2011) 3263.
15. Wang X J, Wang N Z, and Wang L Y, *Mater Des* **57** (2014) 638.
16. Ezatpour H R, Torabiparizi M, and Sajjadi S A, *Mater Chem Phys* **178** (2016) 119.
17. Suresha S, and Sridhara B K, *Compos Sci Technol* **70** (2010) 1652.
18. Mahdavi S, and Akhlaghi F, *J Compos Mater* **47** (4) (2012) 437.
19. Hassan A M, Mayyas A T, Alrashdan A, and Hayajneh M T, *J Mater Sci* **43** (2008) 5368.
20. Kumar S, and Balasubramanian V, *Tribol Int* **43** (2010) 414.
21. Basavarajappa S, Chandramohan G, and Mahadevan A, *Wear* **262** (2007) 1007.
22. Sahin Y, *Tribol Int* **43** (2010) 939.
23. Ravindran P, Manisekar K, Narayanasamy P, Selvakumar N, and Narayanasamy R, *Mater Des* **39** (2012) 42.
24. Radhika N, and Raghu R, *Tribol Lett* **59** (2015) 2.
25. Kok M, *J Adv Manuf Technol* **52** (2010) 207.
26. Chiang K T, *Int J Adv Manuf Technol* **37** (2008) 523.
27. Ranganathan S, and Senthilvelan T, *J Adv Manuf Technol* **56** (2011) 455.
28. Ravi Kumar K, and Sreebalaji V S, *Tribol Mater Surfaces Interfaces* **9** (2015) 128.
29. Gopalakannan S, and Senthilvelan T, *Measurement* **46** (2013) 2705.